Experimental and numerical study of the sloshing motion in a rectangular tank with a perforated screen

B. Molin, F. Remy
École Centrale Marseille & Institut de Recherche sur les Phénomènes Hors Équilibre (IRPHE)
bernard.molin@centrale-marseille.fr, fabien.remy@centrale-marseille.fr

In the past years many papers have appeared on so-called TLDs: Tuned Liquid Dampers. E.g. see Tait *et al.* (2005), Faltinsen & Timokha (2009), or Faltinsen *et al.* (2011). In this last paper the authors present experimental and numerical results on the sloshing motion inside a rectangular tank undergoing forced sway motion. The tank is fitted with a vertical slat screen in its middle and the solidity ratios and numbers of slots are varied. The results shown only deal with the free surface elevation at the wall, no data are given for the added mass and damping coefficients.

Here we report similar experiments, for the same waterdepth - tank width ratio. Our screen consists in a perforated plate. At variance with Faltinsen *et al.* (2011), we keep constant the open-area ratio (18 %) and we vary the imposed motion amplitude. We also present results for the added mass and damping coefficients. Comparisons are shown with a numerical model that assumes linear free surface equations and quadratic discharge law at the screen.

Use was made of an existing tank with internal dimensions: length 80 cm, width 50 cm and height 60 cm. As a matter of fact this is the tank that was used by Molin *et al.* (2002) to study the coupling between sloshing and sea-keeping. To ensure two-dimensional flow and to increase the rigidity of the screens, the tank was subdivided into 4 compartments, lengthwise, about 12 cm wide each.

The perforated screens consisted in 4 steel plates (one per compartment), 2 mm thick, with circular openings of diameter 4 mm (figure 1). The open-area ratio was 18 %.

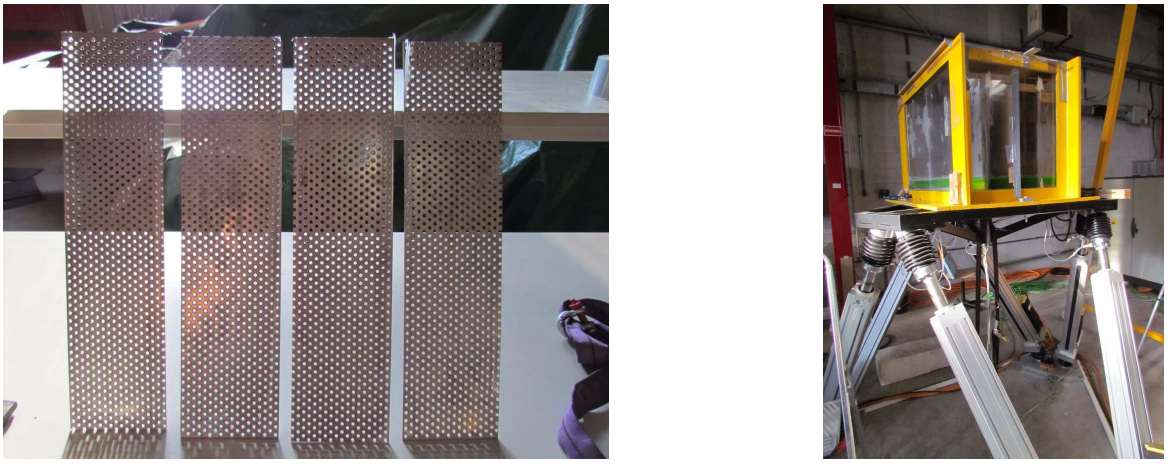

Figure 1: Perforated screens and the tank on the Hexapode (with a different filling condition).

The tank was installed on the Hexapode (see http://www.symetrie.fr/en/) test bench and filled to a waterheight of 32 cm. The free surface elevation at one of the end walls was measured through image processing of video recordings with a camera attached to the Hexapode. To improve optical detection the water was dyed with fluorescein. Our Hexapode is fitted with force sensors which deliver the connecting loads in-between the supporting table and the legs. From the force measurements the added mass and damping coefficients were derived through Fourier analysis.

The numerical model is based on potential flow theory, with the free surface equations linearized. A similar approach is used by Faltinsen *et al.* (2011). The main difference is that we represent the screen as a porous boundary, while Faltinsen *et al.* account for the exact geometry of the slots and slats. Other differences are that we solve the problem in the frequency domain while they use a time domain approach, and that they average the pressure drop over the height of the screen, while we do not.

We take h as the liquid depth and $2b$ as the length of the tank in the y direction. The coordinate system Oyz is centered at mid-tank, with $z = 0$ the undisturbed free surface and $y = 0$, $-h \leq z \leq 0$, the screen. We look for steady-state solution, with the velocity potential written as $\Phi(y, z, t) = \Re\left\{\varphi(y, z)\ \mathrm{e}^{-\mathrm{i}\,\omega\,t}\right\}$. The imposed sway velocity is $v = A\,\omega\ \cos\omega t$.

The velocity potential φ satisfies the Laplace equation in $-b \leq y \leq b\ \ -h \leq z \leq 0$, the linearized free surface equation $g\,\varphi_z - \omega^2\ \varphi = 0$ at $z = 0$, no flow conditions at the solid walls. At the screen the following quadratic discharge equation is written

$$P_- - P_+ = \rho\,\frac{1-\tau}{2\,\mu\,\tau^2}\ V_r\ |V_r| \tag{1}$$

with $P_- - P_+$ the pressure drop, τ the open-area ratio, μ a discharge coefficient (0.5 for the perforated plate), and V_r the relative flow velocity in the normal direction to the perforated screen. See Molin (2011).

The velocity potential is looked for under the form

$$\begin{aligned}\varphi(y,z) \quad &= \quad A\,\omega\ y + \sum_{m=1}^{\infty} A_m\ \cos\lambda_m(y-b)\ \frac{\cosh\lambda_m(z+h)}{\cosh\lambda_m h} \\ &\quad \pm B_0\ \cos k_0(y \pm b)\ \frac{\cosh k_0(z+h)}{\cosh k_0 h} \pm \sum_{n=1}^{\infty} B_n\ \frac{\cosh k_n(y \pm b)}{\cosh k_n b}\ \cos k_n(z+h)\end{aligned} \tag{2}$$

where $\lambda_m = (2\,m-1)\,\pi/(2\,b)$, $A_m = 2\,A\,\omega^3/(\lambda_m^2\ (\omega_m^2 - \omega^2)\ b)$, $\omega_m^2 = g\,\lambda_m\ \tanh\lambda_m h$ and $\omega^2 = g\,k_0\ \tanh k_0 h = -g\,k_n\ \tan k_n h$. Where $\pm$ appears, it means that the $+$ sign is to be used in the left-hand side compartment of the tank and the $-$ sign in the right-hand side. In this way continuity of the horizontal velocity at the screen is ensured. When there is no screen $B_0 \equiv B_n \equiv 0$.

With φ given as (2) the Laplace equation and all boundary conditions are satisfied except for the discharge equation at the porous screen. It writes, after Lorentz linearization:

$$\mathrm{i}\ \omega\ (\varphi_- - \varphi_+) = \frac{4}{3\,\pi}\ \frac{1-\tau}{\mu\,\tau^2}\ \|\varphi_y - A\,\omega\|\ (\varphi_y - A\,\omega) \tag{3}$$

This is satisfied through iterations by writing equation (3) under the form

$$\mathrm{i}\ \omega\ (\varphi_-^{(j)} - \varphi_+^{(j)}) = \frac{4}{3\,\pi}\ \frac{1-\tau}{\mu\,\tau^2}\ \|\varphi_y^{(j-3/2)} - A\,\omega\|\ (\varphi_y^{(j)} - A\,\omega) \tag{4}$$

which leads to

$$\begin{aligned}&B_0^{(j)}\ \left(\cos k_0 b + k_0\ \sin k_0 b\ f^{(j-3/2)}(z)\right)\ \frac{\cosh k_0(z+h)}{\cosh k_0 h} \\ &+\sum_n B_n^{(j)}\ \left(1 - k_n\ \tanh k_n b\ f^{(j-3/2)}(z)\right)\ \cos k_n(z+h) \quad = \quad f^{(j-3/2)}(z)\ g(z)\end{aligned} \tag{5}$$

with

$$g(z) \quad = \quad \sum_m \lambda_m\,(-1)^{(m+1)}\ A_m\ \frac{\cosh\lambda_m(z+h)}{\cosh\lambda_m h} \tag{6}$$

$$f^{(j)}(z) \quad = \quad -\frac{2\,\mathrm{i}}{3\,\pi\,\omega}\ \frac{1-\tau}{\mu\,\tau^2}\ \left\| g(z) - k_0\ B_0^{(j)}\ \sin k_0 b\ \frac{\cosh k_0(z+h)}{\cosh k_0 h} + \sum_n k_n\ B_n^{(j)}\ \tanh k_n b\ \cos k_n(z+h) \right\| \tag{7}$$

In equations (4) and (5) $(j-3/2)$ means that the average values of B_n between the previous two iterations $(j-2)$ and $(j-1)$ are used to compute $f(z)$. In this way relaxation is introduced in the iterative scheme and convergence is faster.

Each side of equation (5) is multiplied by $\cosh k_0(z+h)$ (then $\cos k_n(z+h)$) and integrated in z from $z=-h$ to $z=0$. When the A_m and B_n series are truncated at orders M and N respectively, this provides a linear system of rank $N+1$ which is solved with a Gauss routine. Convergence is reached within 10 to 20 iterations with the B_n coefficients initially taken equal to zero. With $M=N=10$, 4 digits accuracy is obtained in the considered cases. The velocity potential at the wall free surface corner is

$$\varphi(-b,0) = -A\,\omega\,b - \sum_{m=1}^{M} A_m + B_0 + \sum_{n=1}^{N} B_n\,\frac{\cos k_n h}{\cosh k_n b} \tag{8}$$

and the free surface elevation RAO is $\omega\,\|\varphi(-b,0)\|/(A\,g)$. The sway hydrodynamic load is obtained by integrating the dynamic pressure $\mathrm{i}\,\omega\,\rho\,\varphi$ on the solid walls plus perforated screen as

$$F_y = \Re\left\{2\,\mathrm{i}\;\rho\;A\;\omega^2\;b\;h\;(C_a + \mathrm{i}\;C_b)\;\mathrm{e}^{-\mathrm{i}\,\omega\,t}\right\} \tag{9}$$

with

$$\begin{aligned} A\,\omega\,b\,h\,[C_a + \mathrm{i}\;C_b] \;&=\; A\,\omega\,b\,h + \sum_{m=1}^{M} A_m\,\frac{\tanh\lambda_m h}{\lambda_m} \\ &\quad + B_0\;(\cos k_0 b - 1)\;\frac{\tanh k_0 h}{k_0} + \sum_{n=1}^{N} B_n\;\left(1 - \frac{1}{\cosh k_n b}\right)\;\frac{\sin k_n h}{k_n} \end{aligned} \tag{10}$$

C_a being the added mass coefficient and C_b the damping coefficient.

It must be pointed out that, according to our theoretical model, the RAOs of the free surface elevation and the hydrodynamic coefficients depend on the motion amplitude A, the tank length $2\,b$ and the coefficient $(1-\tau)/(2\mu\,\tau^2)$ only through the parameter $A/(2\,b)\;(1-\tau)/(2\mu\,\tau^2)$: it is equivalent to vary the motion amplitude A or porosity τ as long as $A/(2\,b)\;(1-\tau)/(2\mu\,\tau^2)$ is kept constant.

Figures 2 through 4 show the free surface RAOs, added mass and damping coefficients, vs. the frequency ω, for different forced motion amplitudes. The left-hand side column is computations only. As the motion amplitude increases from zero, the curves smoothly evolve from the "no wall" case to the "solid wall" case. In the right-hand side column comparisons are made with experimental values at 2 mm, 6 mm, 10 mm and 14 mm sway amplitudes. The agreement between calculations and measurements is quite good as long as nonlinear free surface effects do not come into play.

A striking feature is that the free surface RAO curves seem to cross exactly at two frequencies close to 7 rad/s and 10.3 rad/s. Likewise the added mass coefficients curves seem to cross each other at the natural frequencies of the first (5.72 rad/s) and second (8.72 rad/s) sloshing modes. Disappointingly, closer inspections reveal that they do not actually cross at the same frequencies.

References

Faltinsen O., Firoozkoohi R. & Timokha A.N. 2011 Steady-state liquid sloshing in a rectangular tank with a slat-type screen in the middle: Quasilinear modal analysis and experiments, *Physics of Fluids*, **23**, 042101.

Faltinsen O. & Timokha A.N. 2009 *Sloshing*, Cambridge University Press.

Molin B. 2011. Hydrodynamic modeling of perforated structures, *Applied Ocean Res.*, **33**, 1–11.

Molin B., Remy F., Rigaud S. & de Jouette J. 2002 LNG-FPSO's: frequency domain, coupled analysis of support and liquid cargo motions, in *Proc. 10th IMAM Conference*, Rethymnon.

Tait M.J., El Damatty A.A., Isyumov N. & Siddique M.R. 2005 Numerical flow models to simulate tuned liquid dampers (TLD) with slat screens, *J. Fluids & Struct.*, **20**, 1007–1023.

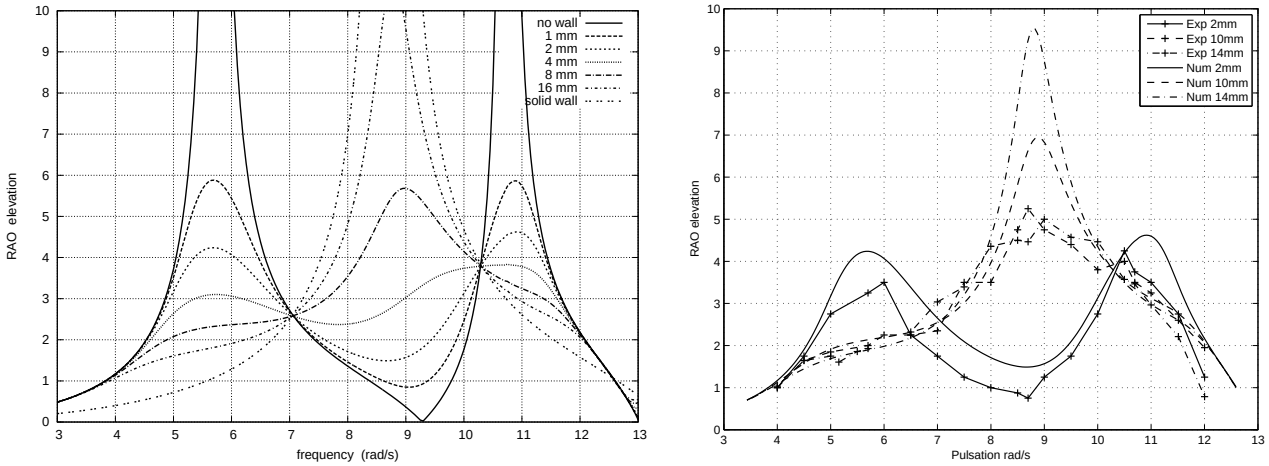

Figure 2: RAO of the free surface elevation at the wall. Results from computations (left) and comparison with the experimental results (right).

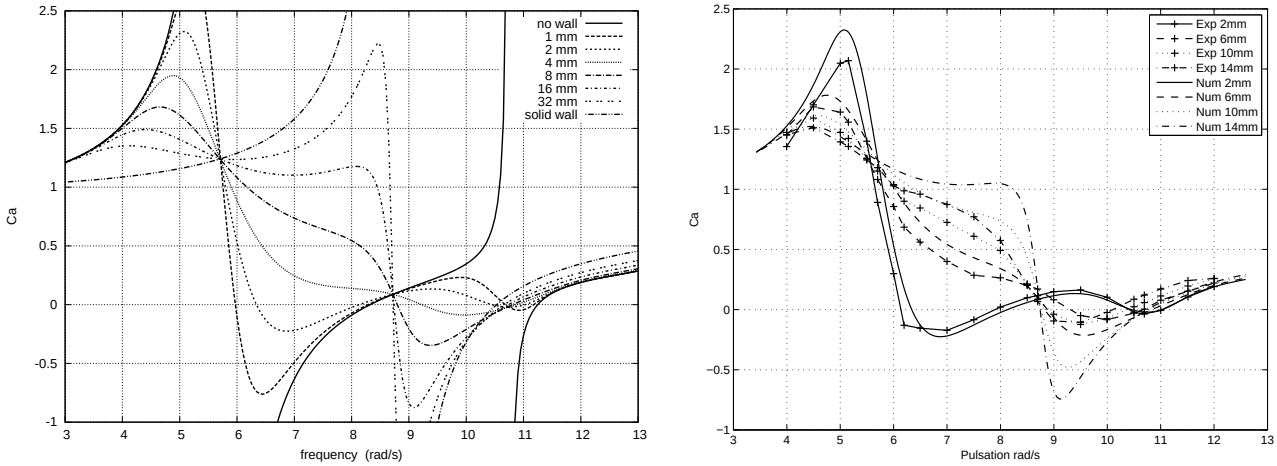

Figure 3: Added mass coefficient. Results from computations (left) and comparison with the experimental results (right).

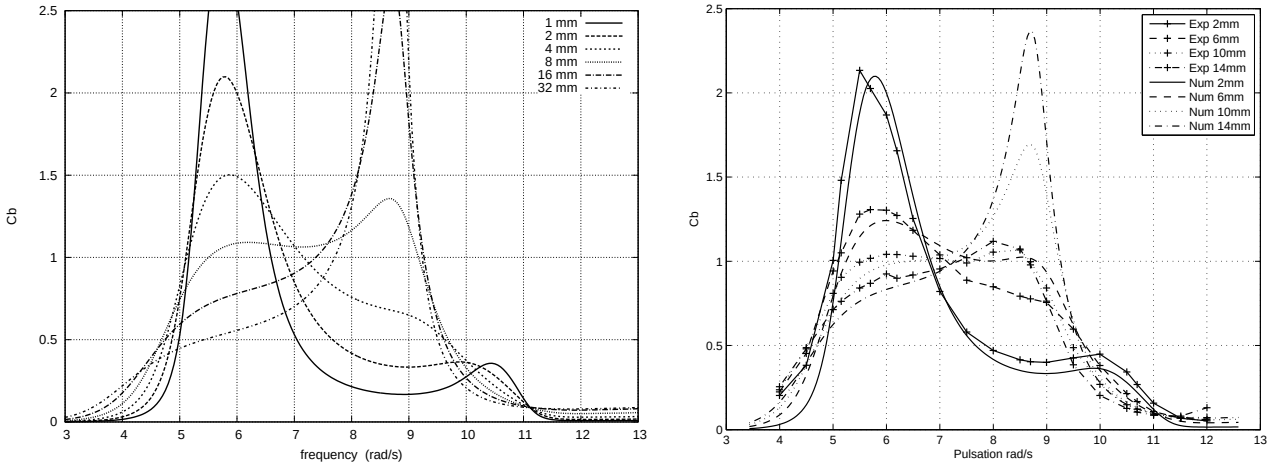

Figure 4: Damping coefficient. Results from computations (left) and comparison with experimental results (right).